Journal of Biological Physics and Chemistry 6 (2006) 125–132

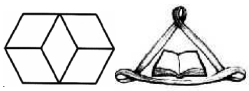

23KO06A

Nano-assembled thin film gas sensors. I. Ammonia detection by a porphyrin-based multilayer film

Serhiy O. Korposh,[1,2,*] Naoki Takahara,[1] Jeremy J. Ramsden,[2,3] Seung-Woo Lee,[1,*] and Toyoki Kunitake[1,4]

[1] *Graduate School of Environmental Engineering, The University of Kitakyushu, 1-1 Hibikino, Kitakyushu 808-0135, Japan*
[2] *Cranfield University Kitakyushu Campus, 1-5-4F Hibikino, Kitakyushu 808-0135, Japan*
[3] *Department of Materials, Cranfield University, MK43 0AL, UK*
[4] *Frontier Research System (FRS), The Institute of Physical and Chemical Research (RIKEN), 2-1 Hirosawa, Saitama 351-0198, Japan*

A thin film of porphyrin deposited by the layer-by-layer method is employed as the active element for an optical sensor. The usefulness of this film technology and the resulting nanoscale matrix for the detection of volatile organic compounds (VOCs), aromatics and amine-containing substances has been studied. The sensing principle is based on monitoring the optical changes of the Q band at 700 nm, as induced by the analyte in the electrostatic interaction between tetrakis(4-sulfophenyl)porphine (TSPP) and poly(diallyldimethylammonium chloride) (PDDA) layers. Three thin film samples with different thicknesses were prepared to assess the effect of film thickness on the sensitivity. For ammonia, the sensor shows a linear sensitivity in the concentration range 0–100 ppm and the sensor response was within 30 seconds. Sensor response could be regenerated by rinsing in distilled water.

Keywords: ammonia detection, layer-by-layer, optical fibres, porphyrin, thin film gas sensor

1. INTRODUCTION

The pollution of outdoor air by industrial activities and mechanized means of transport has caused concern for many years. Governments in many countries have made efforts to protect human health from the effects of air pollution in occupational and general outdoor environments. However, in reality many people nowadays spend most of their time indoors, either in offices or in their homes. Consequently, there is growing concern to understand the effects of pollutants on the indoor environment. This concern is exemplified by the recognition of conditions such as "sick building syndrome".

In 1987 the World Health Organization (WHO) introduced guidelines to help protect public health from the adverse effects of air pollution [1]. Since then, many countries have introduced standards and guidelines for specific pollutants both in the outdoor and indoor air environments. Some countries have produced lists of pollutants and guideline exposure values [2–4] in indoor environments, while others propose using specific indicators of good air quality, rather than defining exposure guidelines [5]. More recently, WHO has updated its "Air Quality Guidelines for Europe" to include indoor pollutants.

To be effective however regulation and standards require the ability to measure accurately and in real time pollutant exposure in both outdoor and indoor environments, especially in relation to the agreed values published in the guidelines. Consequently, much research effort has been applied to the development and creation of low-cost, reliable and robust sensors able to detect environmental gas pollutants [6–10]. A number of different sensor techniques have been employed for the detection of chemical species, based on the measurement of electronic [11], amperometric [12], optical [13] and other physical parameters [10–14]. Optical sensors possess several advantages over other sensor systems and they enable remote, real-time measurements with high sensitivity and selectivity [6].

The key component of an optical sensor is the sensitive element or transducer that converts the chemical recognition step into a detectable optical response that yields a measurable signal. Current research in the field of optical sensors focuses on the creation and development of new sensitive elements that can expand the areas of application and increase the number and range of the analytes measurable by optical sensors [15–18].

Over the past decades the porphyrins and their derivatives have been considered as sensitive elements for electrochemical gas sensors [19], optical sensors [20–23], the quartz crystal microbalance (QCM) [24] and surface acoustic wave (SAW) devices [25], due to their ability to change their optical properties when exposed to various chemical species. Porphyrins are tetrapyrrole pigments, which occur widely in nature and play an important rôle in many biological systems [26]. The optical spectrum of solid state porphyrin is modified

*Corresponding author. Tel.: +81 93 695 3293; fax: +81 93 695 3384. E-mail address: leesw@env.kitakyu-u.ac.jp (S.-W. Lee), S.Korposh@cranfield.jp (S.O. Korposh).

Journal of Biological Physics and Chemistry **6** (2006) 125–132
Received 8 July 2006; *accepted* 29 August 2006

compared to that of porphyrin in solution due to the presence of strong π-π interactions [27]. Interactions with other chemical species can produce further optical spectral changes, thus creating the possibility that they can be applied to optical sensor systems. The high extinction coefficient (> 200 000 $cm^{-1}M^{-1}$) makes porphyrin especially attractive for the creation of optical sensors.

The layer-by-layer method has been shown to be useful for the preparation of molecularly assembled films [28, 29]. It was introduced in 1966 by Iler [30], and subsequently extended by Decher and coworkers to encompass the alternate adsorption of polycations and polyanions onto a surface [31–33]. The technique is still expanding its potential because of its versatility for the fabrication of ordered multilayers.

In this study a thin porphyrin film, deposited by the layer-by-layer method, is employed as the sensitive element for an optical sensor. The usefulness of this film technology and the resulting nanoscale matrix for the detection of amine-containing gaseous substances have been investigated.

Ammonia gas was chosen as a target compound because its sensitive detection is desired but not yet effectively achieved in the environmental, automotive, chemical and medical areas of human activity [34]. Two sensor techniques, optical and the quartz crystal microbalance (QCM), are used to compare the sensitivity, selectivity and reversibility towards different chemical species.

2. EXPERIMENTAL

2.1 Materials

Tetrakis(4-sulfophenyl)porphine (TSPP), poly(sodium 4-styrenesulfonate) (PSS, M_r: 70 000), and poly(diallyldimethylammonium chloride) (PDDA, M_r = 200 000–350 000, 20% $^{w}/_{w}$ in H_2O), (see Scheme 1), were purchased from Tokyo Kasei, Japan. Gelatin (GE, M_r = 30 000) was purchased from Sigma. All of these chemicals were reagents of analytical grade and used without further purification. Deionized pure water (18.3 MΩ cm) was obtained by reverse osmosis followed by ion exchange and filtration in a Nanopure Diamond installation (Barnstead, Ohio).

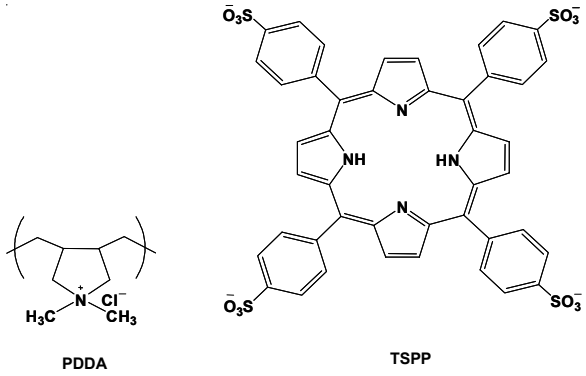

Scheme 1.

2.2 Sample preparation

The electrostatic layer-by-layer (alternating) adsorption method was used for the preparation of three porphyrin thin films of different thicknesses onto quartz plates. A schematic illustration of this method used with oppositely charged PDDA and TSPP is given in Figure 1.

Before the assembly, the quartz plates were cleaned with concentrated sulfuric acid (96%), rinsed several times with deionized water, treated with 1% $^{w}/_{w}$ ethanolic KOH (ethanol/water = 3:2 $^{v}/_{v}$) for a few minutes, rinsed with deionized water, and dried in a stream of nitrogen.

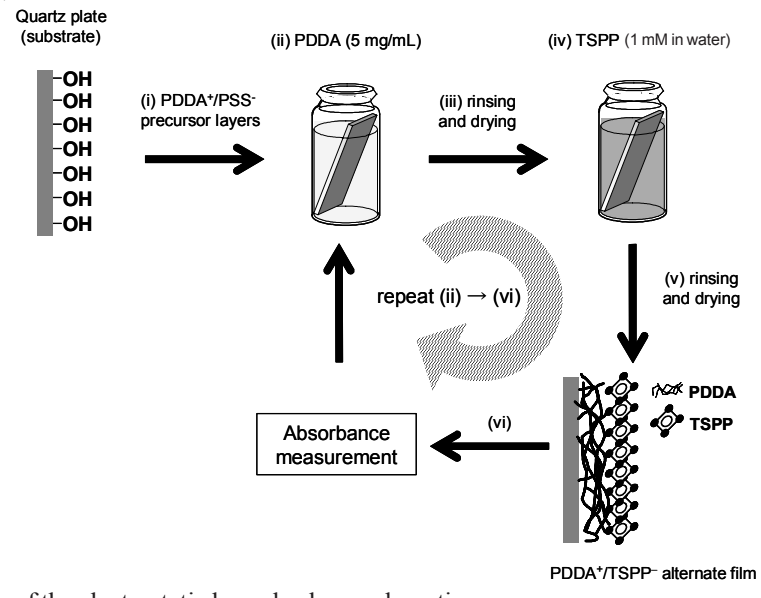

Figure 1. Schematic illustration of the electrostatic layer-by-layer adsorption.

The films were assembled onto such activated quartz plates. In a typical procedure, precursor films were assembled on a quartz plate by repeating three alternate adsorptions of PDDA and PSS. The quartz substrates were alternately immersed for 20 min in aqueous solutions of PDDA (5 mg/mL) and PSS (5 mg/mL), followed by rinsing in pure water and blowing off excess liquid with nitrogen after each immersion. The outermost layer was modified positively to allow the subsequent deposition of the first layer of TSPP. Subsequently, three alternate films of 5, 10 and 15 cycles (one cycle results in a $PDDA^{+}/TSPP^{-}$ bilayer) were prepared by alternate adsorption of PDDA (5 mg/mL in water) and TSPP (1 mM in water) on the quartz plates with an intermediate stage of rinsing with ultrapure water and drying in a stream of nitrogen (see Fig. 1). In every case, the film had an outermost surface of TSPP. The assembly process was monitored by using a JASCO V-570 spectrophotometer to measure the optical absorption.

Additionally, TSPP molecules were immobilized in a gelatin matrix in order to assess matrix effects on sensitivity and selectivity towards ammonia. A 1 mL solution was prepared by mixing 0.5 mL of TSPP (1 mM, 0.1 mM, 0.01 mM and 1 nM) with 0.5 mL of 6% $^{w}/_{v}$ hide-derived gelatin solution. Films were prepared by casting 0.1 mL of the mixed solution onto 2 cm^2 quartz substrates and were allowed to dry for 24 hours under atmospheric conditions prior to measurements.

2.3 Quartz crystal microbalance (QCM) measurements

A quartz crystal microbalance (QCM, 9 MHz) manufactured by USI Systems, Fukuoka, Japan, was used for monitoring layer-by-layer film assembly. Gold-coated quartz resonators were treated with "piranha" solution (96% sulfuric acid: 30–35% hydrogen peroxide, 3:1 $^{v}/_{v}$), rinsed with deionized water, and dried in a stream of nitrogen. They were then immersed in an ethanolic solution of 2-mercaptoethanesulfonate (10 mM) for 12 hours, followed by rinsing with ethanol and drying with nitrogen. The film assembly was carried out onto the 2-mercaptoethanesulfonate-modified gold-coated quartz resonators with the procedure essentially identical to that used for the quartz plates. The mass increase due to adsorption can be estimated from the QCM frequency shift by using the Sauerbrey equation [35]. The following relation between adsorbed mass M and frequency shift ΔF, taking into account the characteristics of the particular quartz resonators used:

$$\Delta F\,/\mathrm{Hz} = -1.832 \times 10^{-8}\,(M\,/\mathrm{g})/(A\,/\mathrm{cm}^2), \qquad (1)$$

where A is the surface area of the resonator (0.159 cm^2). In the system employed for this work, a frequency decrease of 1 Hz corresponds to a mass increase of ca. 0.9 ng.

2.4 Optical measurements

Figure 2 shows a schematic diagram of the experimental apparatus used for the optical measurement. A fibre optic spectrophotometer (Ocean Optics USB2000) was used for monitoring the optical changes induced by the gaseous chemical species that came into contact with the porphyrin film. Optical fibres with a diameter of 400 μm were used for the transporting light to and from the sample holder in which the porphyrin film was fixed. The sample holder was placed in the chamber in which the desired gas concentration could be set up using a two-arm flow system, as shown in Figure 3.

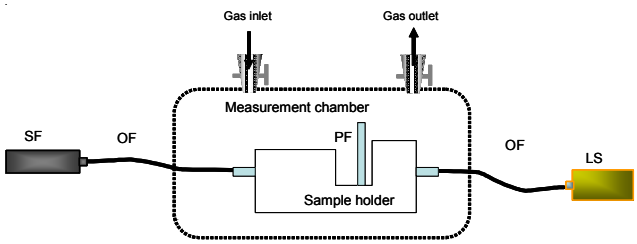

Figure 2. Schematic illustration of the experimental apparatus for investigation of the chemically induced optical changes of the porphyrin film. OF, optical fibres; SF, spectrophotometer; LS, light source; and PF, porphyrin film.

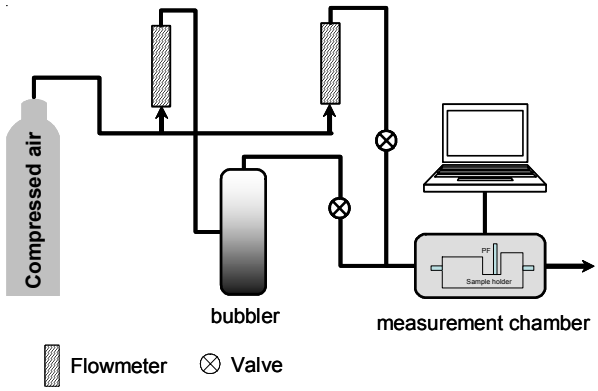

Figure 3. Two-arm flow gas generation system.

Compressed air was used as a carrier gas and passed through a bubbler containing the analytes to be detected, the analyte vapour being in equilibrium with its liquid. Both the bubbler and the measurement chamber were double jacketed and the carrier gas was administered at a flow of 1 L/min. Before each test, a baseline measurement was recorded by passing dry air through the measurement chamber at a flow of 1 L/min.

3. RESULTS AND DISCUSSIONS

3.1 Optical spectra of $PDDA^+/TSPP^-$ alternating films

The assembly of the PDDA and TSPP layers after each deposition cycle was measured by monitoring the absorbance changes and the QCM frequency shifts. In order to determine the wavelength where the biggest changes were observed, the optical spectra in the UV-vis spectral region were recorded. The dynamic changes were monitored at three wavelengths, 425, 486 and 700 nm, corresponding respectively to the first and second Soret and Q absorption bands of the ($PDDA^+/TSPP^-$) film, as shown in Figure 4a. Optical spectra of the ($PDDA^+/TSPP^-$) film are different from that of a TSSP solution in water (Figure 4b). The Q band and Soret bands are shifted towards the red from 645 nm to 700 nm and from 413 to 425 nm, respectively, which can be explained by the formation of J-aggregates of TSPP in the film [33].

The largest absorbance changes due to deposition of the ($PDDA^+/TSPP^-$) bilayer were observed at 425 nm. The absorbance increases in proportion to the number of adsorption cycles up to at least 15 cycles (Figure 4a, inset). Absorbance spectra of the ($PDDA^+/TSPP^-$) films are characterized by a double peak in the Soret band occurring at 425 nm and 485 nm, and by a pronounced peak of the Q band at 700 nm. The double peak in the Soret band is attributed to ordered aggregation of the TSPP moiety [33, 36]. On the other hand, the intensity of the Q band at 700 nm is influenced by the electrostatic interaction with (attraction towards) PDDA. In general, the Q band of a free-base porphyrin is weak because the transition is pseudoparity-forbidden, because of the alternancy symmetry. Hashimoto et al. reported that the Q band in the visible region can be intensified if the pairing property is broken and this is achieved by various chemical modifications to the basic structure of free-base porphyrin, such as adding peripheral substituents, changing the conjugation pathway, and changing the central substituent [37]. This suggests that the symmetric structure of TSPP in the present study can be changed by the electrostatic interaction of TSPP and PDDA layers [38, 39].

Figure 5 shows the frequency shift due to the alternate adsorption of PDDA and TSPP. The frequency decreases linearly with the adsorption cycles, indicating the regular growth of the $PDDA^+/TSPP^-$ multilayer film. Average frequency changes for the adsorption of PDDA and TSPP were 20 ± 9 Hz and 86 ± 21 Hz, respectively. In the current setup, a QCM frequency decrease of 1 Hz corresponds to a thickness increase of 0.233/ρ Å, where ρ (g/cm^3) is the density of the adsorbed film, and we can readily estimate the thicknesses of the PDDA and TSPP

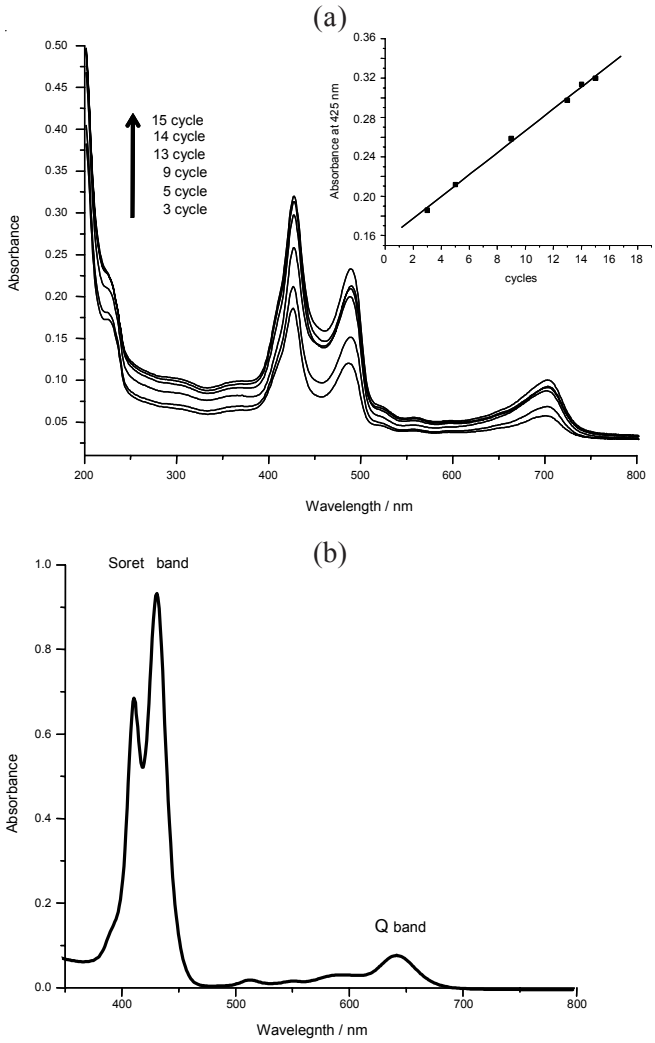

Figure 4. (a) Absorbance changes due to deposition of $PDDA^+/TSPP^-$ bilayers onto a quartz substrate. The inset shows the absorbance change monitored at 425 nm, which corresponds to the Soret band. (b) Absorbance spectrum of an aqueous solution of 1 mM TSPP.

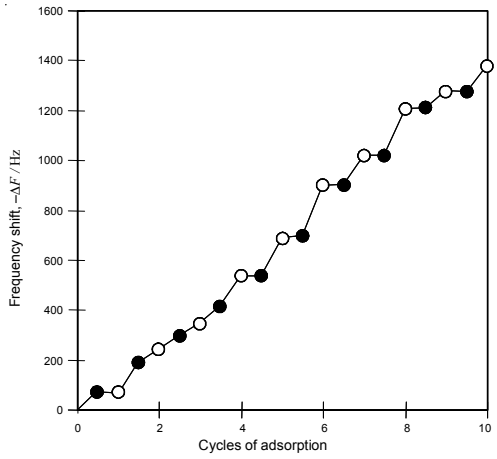

Figure 5. QCM frequency shifts during alternate deposition of $PDDA^+/TSPP^-$ bilayers on a gold-coated quartz resonator. (●), $PPDA^+$ and (○), $TSPP^-$, 5 mg/mL in water and 1 mM in water, respectively.

layers from the ΔF values. Using the density of the polyelectrolyte (1.2 g/cm^3) [38], the ΔF value of 20 ± 9 Hz therefore corresponds to a thickness increase of 5 ± 2 Å for the PDDA layer. Similarly, the thickness of the TSPP layer was calculated to be 18 ± 4 Å from the ΔF value (86 ± 21 Hz) and the bulk density (1.3 g/cm^3) [40]. Therefore, the thickness of the alternate PDDA$^+$/TSPP$^-$ film is estimated to be 23 Å per bilayer.

The UV-vis spectrum of the porphyrin embedded in the gelatin matrix film is shown in Figure 6. In gelatin the absorption spectrum shows features different from those of the solution and the thin film fabricated by alternating adsorption. The Soret band has an absorption band at 419 nm, while the Q band in this structure is characterized by an absorption at 519 nm as compared to 645 and 700 nm in solution and in the (PDDA$^+$/TSPP$^-$)$_{15}$ film, respectively. This can be attributed to the free state of TSPP molecules in the gelatin matrix.

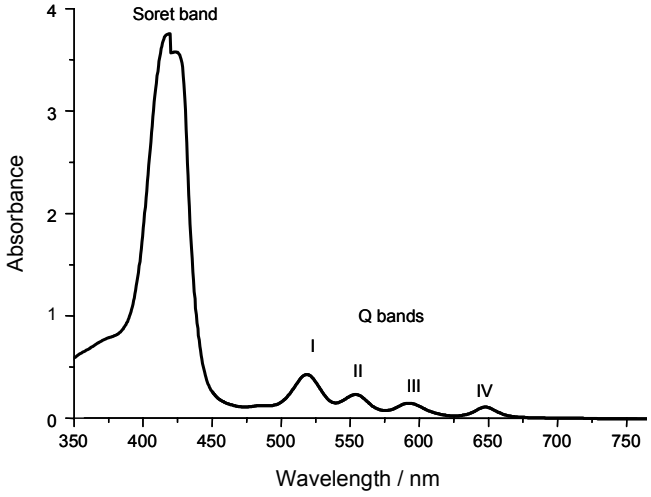

Figure 6. Optical absorption spectra of the porphyrin embedded in a gelatin matrix film.

3.2 Optical response to ammonia

Absorbance changes in the spectrum of the (PDDA$^+$/TSPP$^-$)$_{15}$ film are induced by the presence of ammonia, as shown in Figure 7. As the ammonia concentration increased from 0 to 100 ppm, the absorbances at 485 and 700 nm decreased. Upon exposure of (PDDA$^+$/TSPP$^-$)$_{15}$ film to ammonia, the largest absorbance change was observed at 700 nm, but no changes were observed at 425 nm (1st Soret band). In other words, this result suggests that the absorption of ammonia molecules affects the electrostatic interaction between the TSPP and PDDA layers rather than modulating the ordered structure of TSPP. Dynamic changes of the absorbance of the (PDDA$^+$/TSPP$^-$)$_{15}$ induced by ammonia were monitored at 485 and 700 nm (Figure 8). Sensor response (*S.R.*) is calculated using the following equation:

$$S.R. = \frac{(A_0 - A_{NH_3})}{A_0}, \qquad (2)$$

where A_0 and A_{NH_3} are the absorbances without ammonia and at a given ammonia concentration, respectively. The response time (t_{90}) to increasing ammonia concentrations was always within 30 seconds. The calibration curve was plotted from the recorded spectra at given ammonia concentrations using the absorbance change at 700 nm. The sensor shows a linear response to the ammonia concentration (Figure 9).

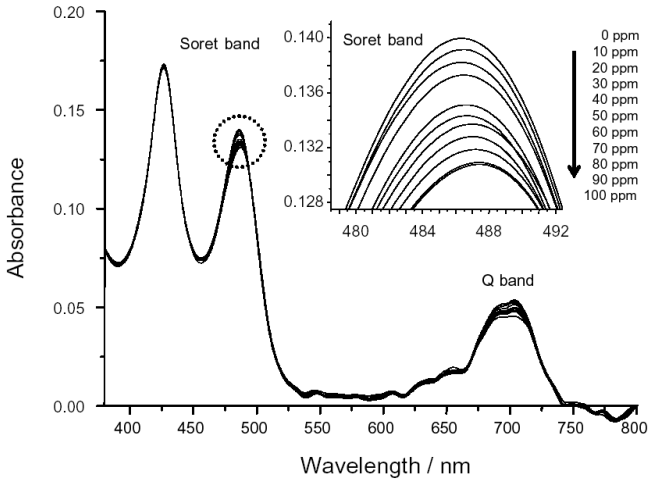

Figure 7. Optical absorption spectra of the (PDDA$^+$/TSPP$^-$)$_{15}$ film measured for ammonia concentration increasing from 0–100 ppm. The inset shows the decrease of the Soret band absorbance (encircled in the main plot) at 485 nm induced by ammonia.

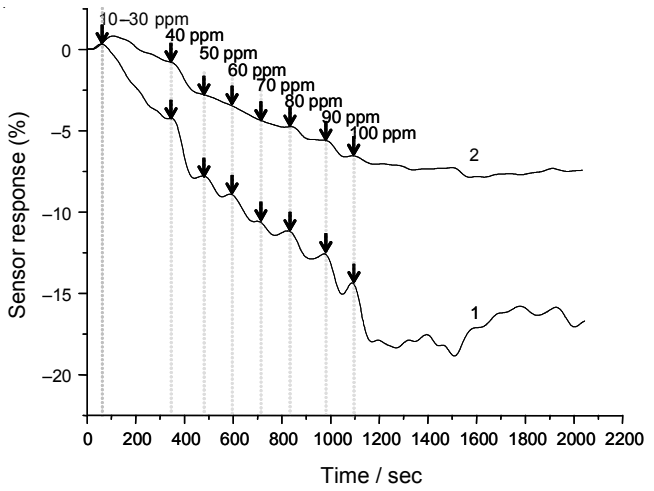

Figure 8. Dynamic responses of the (PDDA$^+$/TSPP$^-$)$_{15}$ films induced by ammonia, monitored at 700 nm (line 1) and 485 nm (line 2).

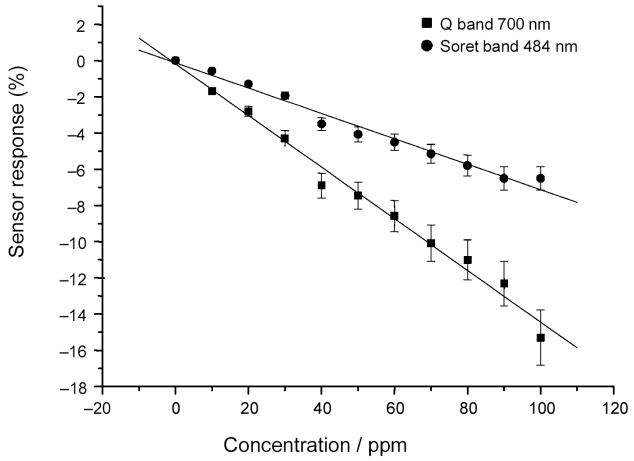

Figure 9. Calibration curves constructed from the spectra recorded at different concentrations of ammonia for the 15 cycle film. Slopes: –0.070 ± 0.003 at 485 nm (filled circles) and –0.143 ± 0.005 at 700 nm (filled squares).

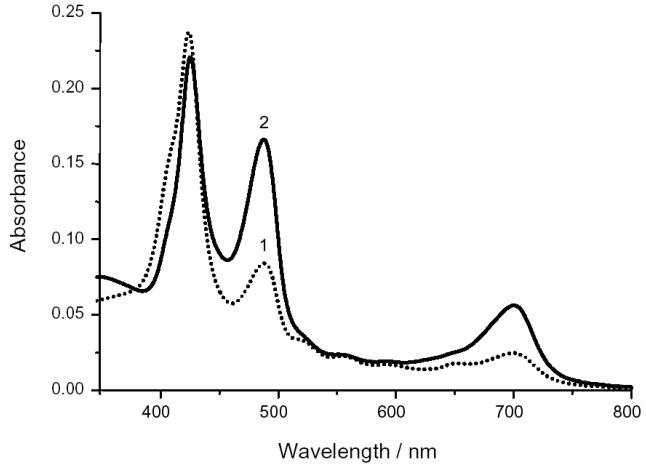

Figure 10. Absorbance spectral changes of the $(PDDA^+/TSPP^-)_{15}$ film after binding ammonia (dotted line 1) and after rinsing in distilled water (solid line 2). See text for more details.

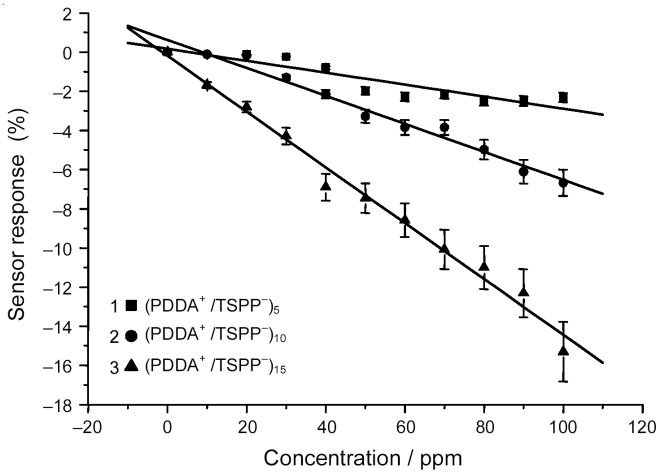

Figure 11. Calibration curves for the $(PDDA^+/TSPP^-)_n$ ($n = 5$, 10, and 15 cycles) films monitored at 700 nm. Slope: –0.030 ± 0.005 ($r = 0.912$, $n = 5$, squares); –0.071 ± 0.004 ($r = 0.988$, $n = 10$, circles); –0.143 ± 0.005 ($r = 0.994$, $n = 15$, triangles).

The ammonia-induced changes were reversible, but the time needed to regenerate the sensor's original absorbance was around one hour, when the measurement chamber was flushed with clean air at a flow of 1 L/min. In order to achieve faster regeneration, the film can be rinsed in distilled water. The absorbance spectra measured after 100 ppm NH_3 exposure for 5 min and after rinsing for a few seconds in distilled water are compared in Figure 10. After rinsing in distilled water, the absorbance decreased at 485 and 700 nm, while no changes at 425 nm were observed. This suggests that ammonia molecules adsorbed on the sensor film can be readily removed.

Three $TSPP^-/PDDA^+$ films of 5, 10 and 15 cycles and porphyrin in a gelatin matrix were exposed to ammonia. The highest sensitivity was observed in the $(PDDA^+/TSPP^-)_{15}$ film (Figure 11). The porphyrin in the gelatin matrix showed no response to ammonia, probably due to the absence of any supramolecular structural features that can be perturbed by electrostatic modulation. The Q band does not play an important rôle in this composite film (see Fig. 6).

4. CONCLUSIONS

Thin solid films of porphyrin were prepared by alternating electrostatic layer-by-layer adsorption, and were used as the sensitive element for the construction of an ammonia optical sensor. The optical response is explained by ammonia-induced changes in the electrostatic interaction between TSPP and PDDA layers, and can be measured by monitoring the absorbance change of the Q-band at 700 nm. Three thin film samples with different thicknesses were prepared in order to assess the dependence of the sensitivity on film thickness. The optical response showed a linear relation at ammonia concentrations of 0–100 ppm and the effective response time was less than 30 seconds. A faster regeneration was achieved by rinsing the film in distilled water after each test.

This work was a first step in the development of a family of fibre-optic gas sensors employing ($PDDA^+$/$TSPP^-$) thin films as the sensitive element for the detection of different gases. The results have demonstrated that detailed investigation of the alternate film structure is required in order to elucidate the sensing mechanism.

ACKNOWLEDGMENTS

This work was supported by the Promotion Programme for Fire and Disaster Prevention Technologies, and the MEXT via the Kitakyushu Knowledge-Based Cluster Project. We are grateful to Prof. William J. Batty for helpful discussions.

REFERENCES

1. *Air Quality Guidelines for Europe*, WHO Regional Publications, European Series, No. 23, Copenhagen: WHO (1987).
2. *Exposure Guidelines for Residential Indoor Air Quality*, Health Canada, Ministry of Supply and Services, Cat H46-2/90-156E (1989).
3. Becher, R., Hongslo, J.K., Bakke, J.V., Kvendbø, J.F., Sanner, T., Schwarze, P.E. & Dybing, E. Revised Guidelines for Indoor Air Quality in Norway. *Indoor Air 1999: Proc. 8th Int. Conf. on Indoor Air Quality and Climate*, Edinburgh, Scotland, vol. 1, pp. 171–176 (1999).
4. Seifert, B., Englert, N., Sagunski, H. & Witten, J. Guideline Values for Indoor Air Pollutants. *Indoor Air 1999: Proc. 8th Int. Conf. on Indoor Air Quality and Climate*, Edinburgh, Scotland, vol. 1, pp. 499–504 (1999).
5. Air Quality Guidelines for Europe, 2nd edn, WHO Regional Publications, European Series, No. 91, Copenhagen: WHO (2000).
6. Grattan, K.T.V. & Meggitt, B.T. *Chemical and environmental sensing*, Dordrecht; Boston: Kluwer, pp. 336 (1999).
7. Zampolli, S., Elmi, I., Ahmed, F., Passini, M., Cardinali, G.C., Nicoletti, S. & Dori, L. An electronic nose based on solid state sensor arrays for low-cost indoor air quality monitoring applications. *Sensors Actuators B* **101** (2004) 39–46.
8. Kessick, R. & Tepper, G. Electrospun polymer composite fiber arrays for the detection and identification of volatile organic compounds. *Sensors Actuators B* **117** (2006) 205–210.
9. Ricco, A., Xu, C., Allred, R., Crooks, R. SAW chemical sensor arrays using new thin-film materials. SAND94-0241C, Albuquerque Sandia National Laboratories, (1994).
10. Ho, C. K., Robinson, A., Miller, D.R. & Davis, M.J. Overview of sensors and needs for environmental monitoring. *Sensors* **5** (2005) 4–37.
11. Winquist, F., Bjorklund, R., Krantz-Rülcker, C., Lundström, I., Östergren, K. & Skoglund, T. An electronic tongue in the dairy industry. *Sensors Actuators B* **111–112** (2005) 299–304.
12. Knake, R., Jacquinot, P., Hodgson, A.W.E. & Hauser, P.C. Amperometric sensing in the gas phase. *Anal. Chim. Acta* **549** (2005) 1–9.
13. Kermani, B.G., Fomenko, I., Kotseroglou, T., Forood, B., Clark, L., Barker, D. & Lebl, M. Decoding beads in a randomly assembled optical nose. *Sensors Actuators B* **117** (2006) 282–285.
14. Lin, H.-B. & Shih, J.-S. Fullerene C60-cryptand coated surface acoustic wave quartz crystal sensor for organic vapors. *Sensors Actuators B* **92** (2003) 243–254.
15. Munkholm, C., Walt, D.R. & Milanovich, F.P. A fibre-optic sensor for CO2 measurement. *Talanta* **35** (1988)100–112.
16. Bariani, C., Matias, I.R., Romeo, I., Garrido, J. & Laguna, M. Behavioral experimental studies of a novel vapochromic material towards development of optical fiber organic compound sensor. *Sensors Actuators B* **76** (2001) 25–31.
17. Grady, T., Butler, T., MacCraith, B.D., Diamond, D. & McKervey, A.M. Optical sensor for gaseous ammonia with tunable sensitivity. *Analyst* **122** (1997) 803–806.
18. Malins, C., Doyle, A., MacCraith, B. D., Kvasnik, F., Landl, M., Šimon, P., Kalvoda, L., Lukaš, R., Pufler, K. & Babusik, I. Personal ammonia sensor for industrial environments. J. *Environmental Monitoring* **1** (1999) 417–422.
19. Lvova, L., Paolesse, R., Di Natale, C. & D'Amico, A. Detection of alcohols in beverages: an application of a porphyrin-based electronic tongue. *Sensors Actuators B* **118** (2006) 439–447.
20. Umar, A.A., Salleh, M.M. & Yahaya, M. Influence of surface microstructure on optical response of ruthenium porphyrins thin films gas sensor. *Eur. Phys. J. Appl. Phys.* **29** (2005) 215–221.
21. Morales-Bahnik, A., Czolk, R. & Ache, H.J. An optochemical ammonia sensor based on immobilized metalloporphyrins. *Sensors Actuators B* **18–19** (1994) 493–496.
22. Spadavecchia, J., Ciccarella, G., Siciliano, P., Capone, S. & Rella, R. Spin-coated thin films of metal porphyrin-phthalocyanine blend for an optochemical sensor of alcohol vapours. *Sensors Actuators B* **100** (2004) 88–93.
23. Papkovsky, D.B. Luminescent porphyrins as probes for optical (bio)sensors. *Sensors Actuators B* **11** (1993) 293–300.
24. Paolesse, R., Di Natale, C., Macagnano, A., Davide, F., Boschi, T. & D'Amico, A. Self-assembled monolayers of mercaptoporphyrins as sensing material for quartz crystal microbalance chemical sensors. *Sensors Actuators B* **47** (1998) 70–76.
25. Di Natale, C., Paolesse, R., Macagnano, A., Mantini, A., Goletti, C. & D'Amico, A. Characterization and design of porphyrins-based broad selectivity chemical sensors for electronic nose applications. *Sensors Actuators B* **52** (1998) 162–168.
26. Kadish, K. M., Smith, K.M. & Guilard, R. *The Porphyrin Handbook*, vol. 11–20 pp. 3500. San Diego: Academic Press (2003).
27. Schick, G.A., Schreiman, I.C., Wagner, R.W., Lindsey, J.S. & Bocian, D.F. Spectroscopic characterization of porphyrin monolayer assemblies. *J. Am. Chem. Soc.* **111** (1989) 1344–1350.
28. Ichinose, I., Fujiyoshi, K., Mizuki, S., Lvov, Y. & Kunitake, T. Layer-by-layer assembly of aqueous bilayer membranes on charged surfaces. *Chem. Lett.* **25** (1996) 257–258.
29. Lee, S.-W., Ichinose, I. & Kunitake, T. Molecular imprinting of azobenzene carboxylic acid on a TiO_2 ultrathin film by the surface sol-gel process. *Langmuir* **14** (1998) 2857–2863.
30. Iler, R.K. Multilayers of colloidal particles. *J. Colloid Interface Sci.* **21** (1966), 569–594.
31. Decher, G. & Hong, J.D. Buildup of ultrathin films by a self-assembly process: Consecutive adsorption of anionic and cation bipolar amphiphiles and polyelectrolytes on charged surface. *Ber. Bunsenges. Phys. Chem.* **95** (1991) 1430–1434.
32. Lvov, Y., Decher, G. & Möhwald, H. Assembly, Structural characterization and thermal behavior of layer-by-layer deposited ultrathin films of polyvinylsulfonate and polyallylamine. *Langmuir* **9** (1993) 481–486.
33. Ramsden, J.J., Lvov, Yu. A. & Decher, G. Optical and X-ray structural monitoring of molecular films assembled via alternate polyion adsorption. *Thin Solid Films* **254** (1995) 246–251; *ibid.* **261** (1995) 343–344.
34. Timmer, B., Olthuis, W. & Van den Berg, A. Ammonia sensors and their applications—a review. *Sensors Actuators B* **107** (2005) 666–677.
35. Ichinose, I., Kawakami, T. & Kunitake, T. Alternate molecular layers of metal oxides and hydroxyl polymers

prepared by the surface sol-gel process. *Adv. Mater.* **10** (1998) 535–539.

36. Snitka, V., Rackaitis, M. & Rodaite, R. Assemblies of TPPS4 porphyrin investigated by TEM, SPM and UV-vis spectroscopy. *Sensors Actuators B* **109** (2005) 159–166.
37. Hashimoto, T., Choe, Y.-K., Nakano, H. & Hirao, K. Theoretical study of the Q and B bands of free-base, magnesium, and zinc porphyrins, and their derivatives. *J. Phys. Chem. A* **103** (1999) 1894–1904.
38. Ariga, K., Lvov, Y. & Kunitake, T. Assembling alternate dye-poluion molecular films by eloctrastatic layaer-by-layer adsorption. *J. Am. Chem. Soc.* **119** (1997) 2224–2231.
39. Gregory van Patten, P., Shreve, A.P. & Donohoe, R.J. Structural and photophysical properties of a water-soluble porphyrin associated with polycations in solutions and electrostatically-assembled ultrathin films. *J. Phys. Chem. B* **104** (2000) 5986–5992.
40. Lvov, Y., Ariga, K., Ichinose, I. & Kunitake, T. Formation of ultrathin multilayer and hydrated gel from montmorillonite and linear polycations. *Langmuir* **12** (1996) 3038–3044.